Composites & nanocomposites

Tailor-made dual doping for morphology control of polyaniline chains in cellulose nanofiber-based flexible electrodes: electrical and electrochemical performance

Tereza Bautkinová[1], Petr Mazúr[1], Gabriela Soukupová[1], Marcela Dendisová[1], Jan Prokeš[2], Marek Jurča[3], Dušan Kopecký[1], Miloslav Lhotka[4], Pavel Ulbrich[5], and Fatima Hassouna[1,*]

[1] *Faculty of Chemical Engineering, University of Chemistry and Technology, 166 28 Prague 6, Prague, Czech Republic*

[2] *Faculty of Mathematics and Physics, Charles University, 180 00 Prague 8, Czech Republic*

[3] *Centre of Polymer Systems, Tomas Bata University in Zlín, 760 01 Zlín, Czech Republic*

[4] *Faculty of Chemical Technology, University of Chemistry and Technology, 166 28 Prague 6, Prague, Czech Republic*

[5] *Faculty of Food and Biochemical Technology, University of Chemistry and Technology Prague, 166 28 Prague 6, Czech Republic*

ABSTRACT

The present study revealed the effect of combining one strong-inorganic and weak-organic protonic acid dopants on the electrical conductivity and electrochemical properties of flexible free-standing composite electrodes based on polyaniline and nanofibrillated cellulose (NFC) or its carboxylated analog (CNFC), synthesized using a bottom-up approach. Hydrochloric acid (HCl) served as a low molecular weight inorganic dopant while phytic acid (PhA) and poly(2-acrylamido-2-methyl-1-propanesulfonic acid) (PAAMPSA) were chosen as the organic dopants. Both PhA and PAAMPSA acted as secondary dopants in the dually doped composites through the molecular conformation changes of PANI chains. Synergistic increase in the electrical conductivity is observed for dually doped PANI-NFC with the combination of PAAMPSA and HCl in comparison with PhA and HCl. Unlike the PhA, the morphological changes induced by PAAMPSA are more favorable for the enhancement of conductivity. Neither the morphological changes, nor the carboxylation of NFC affected the electrochemical properties of the composites as the specific capacitance values were influenced mainly by the type and the strength of the individual acids. The capacitance values per gram of the dually doped composite with PAAMPSA and HCl increased with the decrease in the NFC or CNFC loading reaching values above 200 $F \cdot g^{-1}$ measured at 50 $mV \cdot s^{-1}$ of composite for the 80 wt% PANI content. These results highlight the profound impacts of the secondary dopant in PANI on the performance of PANI-based nanocellulose composites.

🌢 Springer

Introduction

With the rapid increase in energy and power demands for the next-generation of flexible and portable electronics like wearable devices, roll-up displays and photovoltaic cells, considerable efforts have been made to explore flexible, low-cost, lightweight, environmentally friendly and high-performance sustainable energy storage devices [1, 2]. Substitution of conventional materials in the fabrication of energy storage devices by renewable materials has been encouraged to tackle issues related to the dependence on fossil fuels and their negative impact on the environment. In this regard, cellulose is the most abundant natural polymer on Earth [3]. Compared to regular cellulose substrates, nano-structured cellulose, namely nanofibrillated cellulose (NFC), cellulose nanocrystals and bacterial cellulose, exhibits higher mechanical strength, high aspect ratio, low density, better optical transparence, and smoother and more reactive surface with the potential for tunable functionalization. Those features make the nanocellulose an attractive choice for various applications [4, 5]. It can be employed as a matrix for fabrication of flexible composites with some active materials that are intrinsically rigid or brittle. A good example of such brittle materials is electrically conducting polymers (ECP). ECPs like polyaniline (PANI) have developed into a promising category of materials for energy storage devices thanks to their relatively high theoretical capacities (~ 100 to 140 mA·h·g^{-1}), rich redox chemistry, versatility as well as lightweight and inexpensiveness [1, 6, 7]. Nevertheless, because of their poor mechanical properties and processability (infusibility and limited solubility in all available solvents), it is very difficult to produce neat ECP films. Flexible free-standing electrically conductive films based on NFC and PANI are very attractive materials for development of high-performance sustainable energy storage devices [8, 9]. Electrical conductivity and supercapacitive behavior of PANI can be influenced by the nature of the dopant [10, 11]. Doping can be performed by two routes, namely i) redox doping, in which oxidizing or reducing agent add/remove electron to/from polymeric backbone, or ii) protonic acid doping, in which the electron number in the polymer backbone stays unaffected [11]. Recent studies showed that in addition to the utilization of an individual (i.e., single) dopant, a secondary doping, as well as the use of dopant combination, can significantly enhance the electrical and electrochemical properties of PANI [10–12]. The primary dopant, which can be a molecule or a macromolecule, is capable of changing drastically the electronic, magnetic, optic or/and structural properties of PANI, and leads to a substantial increase in the electrical conductivity [12]. On the other hand, the secondary dopant is an apparently inert molecule (e.g., solvent) which can positively affect the above-mentioned properties and is accompanied with further enhancement of the electrical conductivity of PANI, even after a complete removal of the secondary dopant. In some cases, it can also further enhance the electrochemical properties [10–14]. MacDiarmid et al. demonstrated that the impacts of the secondary dopants are based mainly on the molecular conformation changes of PANI from compact coil to expanded coil [12]. Secondary doping of PANI during the synthesis with different combinations of primary/secondary dopant such as sulfophthalic acid/sodium laurylsulfate [15], fluoroboric acid/dodecylhydrogen sulfate [16], hydrochloric acid (HCl)/sodium dodecyl sulfate [17], HCl/polyacrylic acid [17] and camphorsulfonic acid/citric acid [10] has been reported in several studies. They have all reported an enhancement of the electrical conductivity properties of doped PANI. Interestingly, apparently inert solvents like m-cresol can also act as a secondary dopant for PANI following similar mechanism of the secondary doping process described above [12]. For instance, it has been reported that a solvent casted camphorsulfonic acid-doped PANI using m-cresol (solvent) exhibited 10^3 times higher electrical conductivity than the cast obtained from chloroform [12]. Establishment of polar interactions between the polar m-cresol and the polar chains of PANI promotes an expanded open coil conformation of PANI chains.

Despite these considerable scientific efforts made to enhance the properties of PANI and to understand the synergetic effect mechanism of the simultaneous dual doping, secondary doping of PANI in complex systems involving more than one component, i.e., composites, has been barely investigated. According to the available literature, secondary doping has not been explored in flexible free-standing electrically conductive electrodes based on nanocellulose and PANI yet despite the tremendous interest aroused in these materials. The present study reveals the effect

of the combinations of one strong-inorganic and weak-organic protonic acid dopants on the electrical and electrochemical properties of composite electrodes based on PANI and NFC or its carboxylated NFC (CNFC). To the best of our knowledge, this is the first study, which explored the effect of the dual doping, with the objective to improve the electrical and electrochemical performance of the free-standing NFC-based composites. The composite electrodes were prepared using a bottom-up approach as free-standing flexible films. HCl was selected as a low molecular weight inorganic dopant that is known to yield PANI with high values of electrical conductivity [18]. Phytic acid (PhA) and poly(2-acrylamido-2-methyl-1-propanesulfonic acid) (PAAMPSA) were chosen as organic acid dopants. PhA can act as a dopant as well as a crosslinker of PANI thanks to the multiple phosphoric acid groups present in its backbone [19, 20]. Unlike PhA, PAAMPSA is a polymeric dopant of PANI formed via polymerization of 2-acrylamido-2-methyl-1-propanesulfonic acid (AAMPSA). PAAMPSA induces uniform crystalline nanofibrillar morphology of PANI chains [21]. A combination of the benefits of these two types of doping acids, namely desired and controlled morphological features provided by organic acids (PhA or PAAMPSA) and high electrical conductivity provided by inorganic acid (HCl), was explored with the goal to optimize the electrical and electrochemical performance of the final PANI/NFC and PANI/CNFC composite films. The impact of the surface chemistry of the cellulosic fibers (i.e., hydroxyl groups in NFC and carboxyl groups in CNFC) and the composite composition on the structural and morphological features are related performance of the dually doped PANI-based composites was also investigated.

Experimental part

Materials

Nanofibrillated cellulose (NFC) was kindly donated by Weidmann Fiber Technology. Aniline (ACS reagent, > 99.5%), 2-acrylamido-2-methyl-1-propanesulfonic acid (AAMPSA, 99%), sulfuric acid (H_2SO_4, 95–98%), phytic acid (PhA, 50 wt% solution in water), ammonium persulfate (APS, 98%), 2,2,6,6-Tetramethylpiperidine-1-oxyl radical (TEMPO, 98%),

sodium hypochlorite solution (NaClO, 10 wt%), sodium bromide (NaBr) and dimethyl sulfoxide (DMSO) were purchased from Sigma Aldrich. Fuming hydrochloric acid (HCl, 37%) was purchased from Merck. All chemicals were used as received without any further purification. All aqueous solutions were prepared using deionized water.

Materials preparation

Synthesis of PANI with various doping acids

Synthesis of PANI was carried out by chemical oxidative route in the presence of one or two acids for individual and dual doping, respectively. Acids, namely HCl, PhA, PAAMPSA (via polymerization of AAMPSA), PhA/HCl and PAAMPSA/HCl were used. In a typical PANI synthesis, 300 mg of aniline was dissolved in 60 mL of an aqueous solution of a particular acid(s), to keep the concentration of PANI constant at 0.5 wt% regardless of the doping agent(s) used. The proportions in molar ratios of aniline/organic co-dopant (i.e., PhA and AAMPSA) in the dually doped samples were set to 1:1. Table S1 in the supporting information summarizes the sample designations together with amount of acid(s) dissolved in the reaction medium. The reaction system was cooled down in an ice bath prior to the dropwise addition of 5 mL of APS aqueous solution (0.15 w/w%) to initiate the chemical reaction. The reaction mixture was stirred at 300 rpm overnight. The resulting PANI in a form of dark green precipitate was then filtered and washed several times with deionized water, and subsequently dried at room temperature for several days to obtain dry powder. The PANI powders were labeled as PANI(dopant) or PANI(co-dopant + dopant) (Table S1).

Synthesis of PANI-NFC composites with various doping acids

The synthesis of individually and dually doped PANI-NFC composites was performed following the same experimental protocol than for PANI powders, with slight modifications. For PANI-NFC composites, 300 mg of NFC and 300 mg of aniline (weight ratio aniline/NFC = 50:50 w/w%) were incorporated in 120 mL aqueous solution of a particular acid(s), adjusting the concentration of PANI-NFC at 0.5 wt% regardless of the employed doping agent(s). Stirring

speed was increased to 600 rpm to overcome the higher viscosity caused by the addition of NFC. Table S1 summarizes the sample designations together with amount of acid(s) dissolved in the reaction medium. The reaction system was cooled down in an ice bath prior to the dropwise addition of 5 ml of APS aqueous solution (0.15 wt%). The reaction mixture was stirred at 600 rpm overnight. After the polymerization was completed, the resulting green dark precipitate was washed several times. The washed product was resuspended in 70 mL of deionised water by sonication for 10 min using sonication bath (PS 3000, PowerSonic). Afterward, the suspension was casted on a glass mold with defined shape. The concentration of PANI in the films was set to 2 mg·cm^{-2}. The casted materials were dried at room temperature for several days to obtain free standing films with the weight ratio PANI/NFC of 50:50 w/w%. The composites were labeled as PANI(-dopant)-NFC or PANI(co-dopant + dopant)-NFC (Table S1).

Synthesis of PANI-NFC composites at different PANI/NFC ratio

The synthesis of dual-doped PANI(PAAMPSA + HCl)-NFC composites at various PANI:NFC ratios was performed following the synthetic route described above (see Section "Synthesis of PANI-NFC composites with various doping acids"). The amount of NFC was varied while that of aniline was kept constant (300 mg). The amount of AAMPSA was also kept constant (600 mg) and the volume of 1 M HCl aqueous solution was adjusted for each composite (see Table S1). The sample designations are shown in Table S1 where the ratio in w/w% of PANI(-PAAMPSA + HCl):NFC is denoted at the end of the sample name.

Synthesis of CNFC and their PANI-based composites

CNFC was synthesized by TEMPO mediated oxidation of NFC [22]. 510 mg of NFC was dispersed in 100 mL of deionized water, and 14.75 mg of TEMPO and 162 mg of NaBr dissolved in 5 mL of deionized water were added. NaOH solution (0.5 M) was used to maintain pH 10.2 all over the reaction. 7 mL of NaClO was then added to initiate the oxidation. The reaction was quenched after 60 min by addition of 2 mL of methanol. The resulting CNFC was washed

several times with deionised water in a centrifuge (10,000 rpm for 5 min). The concentration of -COOH groups obtained by conductometric titration was 1.56 mmol·g^{-1}.

The synthesis of dual-doped PANI(PAAMPSA + HCl)-CNFC composites at various PANI:CNFC ratios was carried out following the synthetic route used to prepare PANI(PAAMPSA + HCl)-NFC (see Section "Synthesis of PANI-NFC composites at different PANI/NFC ratio").

Characterization methods

Dispersive Raman spectrometer

Dispersive Raman spectrometer with the microscope InVia Reflex was employed for chemical characterization of samples. Excitation wavelength 785 nm with laser power of 2 mW was used. Ten accumulations taking 30 s were recorded for one acquisition and final spectrum is average of 10 acquisitions.

X-ray photoelectron spectroscopy

X-ray photoelectron spectroscopy analysis was carried out with Omicron Nanotechnology X-ray photoelectron spectroscope (XPS) composed of monochromatic radiation of Al lamp (1486.7 eV) in constant analyzer energy mode. Deconvolution of collected spectra was done using CasaXPS software.

Scanning electron microscopy

Surface and bulk morphology of the films was analyzed using thermo-autoemission scanning electron microscope (SEM) Mira 3 LMH (Tescan Orsay) under 3 kV of accelerating voltage.

Transmission electron microscopy

The morphology of NFC and CNFC at a nanoscale level was analyzed using transmission electron microscope (TEM) 100 kV, model JEM-1010 (JEOL, Ltd.) equipped with CCD camera MegaView III (Olympus Soft Imaging Systems). In short, 10 μL of suspension was deposited on a carbon-coated electron microscopic grid. Sample contrasting was performed using 1 wt% uranyl acetate. The grid was dried and then was introduced into the electron microscope column for analysis.

Electrical conductivity

Room temperature electrical conductivity was determined by a four-point method in van der Pauw arrangement using a Keithley 220 Programmable Current Source, a Keithley 2010 Multimeter as a voltmeter and a Keithley 705 Scanner equipped with a Keithley 7052 Matrix Card. Films were analyzed as prepared, while reference PANI powders were finely grinded and then pressed into pellets with a pressure of 527 MPa for a duration of 5 min. Digital micrometer was used to measure sample thickness before the electrical conductivity measurement. Values of conductivities are provided with approx. 5% accuracy.

Electrochemical characterization

The electrochemical properties were tested in 1 M H_2SO_4 electrolyte. A mercury sulfate reference electrode (MSE) with saturated K_2SO_4 inner electrolyte (0.65 V vs. SHE) and platinum sheet counter electrode were used in a three-electrode arrangement. The electrochemical behavior of the nanocomposites was characterized by cyclic voltammetry (CV) in potential range from $- 0.1$ to 0.5 V vs. MSE with scan rate of 50 mV·s^{-1} and by galvanostatic charging discharging (GCD) at various constant currents. Potentiostat/galvanostat/FRA EC-LAB SP-300 (Biologic) is used for these measurements.

The specific capacitance is evaluated from CV experiment following formula 1:

$$C_{sp} = \frac{\int_{E_{\min}}^{E_{\max}} \frac{I}{v} dE}{(E_{\max} - E_{\min}) \cdot m} \tag{1}$$

where v is scan rate, m is mass of electrochemically active components in the material, and $E_{\max}$ and $E_{\min}$ are the chosen boundaries of the integral. Herein, specific capacitance is calculated from cathodic part of CV curve within boundaries from –0.8 V to 0.2 V vs. MSE. The samples were measured in a form of small circles, 6 mm in diameter. Mass of these circles varied from 1 to 2 mg, depending on specific sample.

GCD experiments that were used for establishment of cycling stability of prepared composites were done at controlled current of 2 mA (corresponding to current density of 0.64 mA·cm^{-2}) in a narrower voltage window from $- 1$ to 0.1 V vs. MSE in order to avoid hydrolysis of PANI.

Tensile testing

Mechanical properties of the composite films were evaluated by tensile tests. Five specimens (20 × 5 mm) were cut from each sample. A micrometer was used to measure their thickness before the test. Measurements were taken at four different positions for each specimen, and the average value was used for the calculation. Tensile test was performed using a universal testing machine (EZ graph, Shimadzu Corporation) with a 100 N load cell and a 0.5 mm·min^{-1} strain rate.

Nitrogen physisorption

The specific surface area (S_{BET}) was measured on a 3Flex analyzer (Micromeritics, Norcross) using the gas sorption technique. The samples were degassed at 373 K (12 h) prior to N_2 adsorption analysis, in order to obtain a clean surface. The adsorption isotherms were fitted by using the Brunauer–Emmett–Teller (BET) method for specific surface area.

Results and discussion

PANI-NFC composites doped with different acids

All PANI-NFC composites doped with different acids are dark green films with a thickness of approx. 70 μm. Representative photographs of PANI-NFC composite films are shown in Fig. 1. All films are mechanically stable and can be rolled up without breaking.

Chemical structure and morphology

Chemical structure of the reference PANI powders and PANI-NFC composite films (Fig. 1) doped with various acids was examined by means of Raman spectroscopy and XPS.

Raman spectra of all PANI powders depicted in Fig. 2a display the characteristic peaks corresponding to the structure of emeraldine salt, typically at 1510 cm^{-1} (vibrations of N–H in semiquinonoid structures), 1345 cm^{-1} (C–N^{+} vibrations of delocalized polarons), 1175 cm^{-1} (C–H bending in

Figure 1 Representative photographs of PANI-NFC composite films prepared with various doping acids.
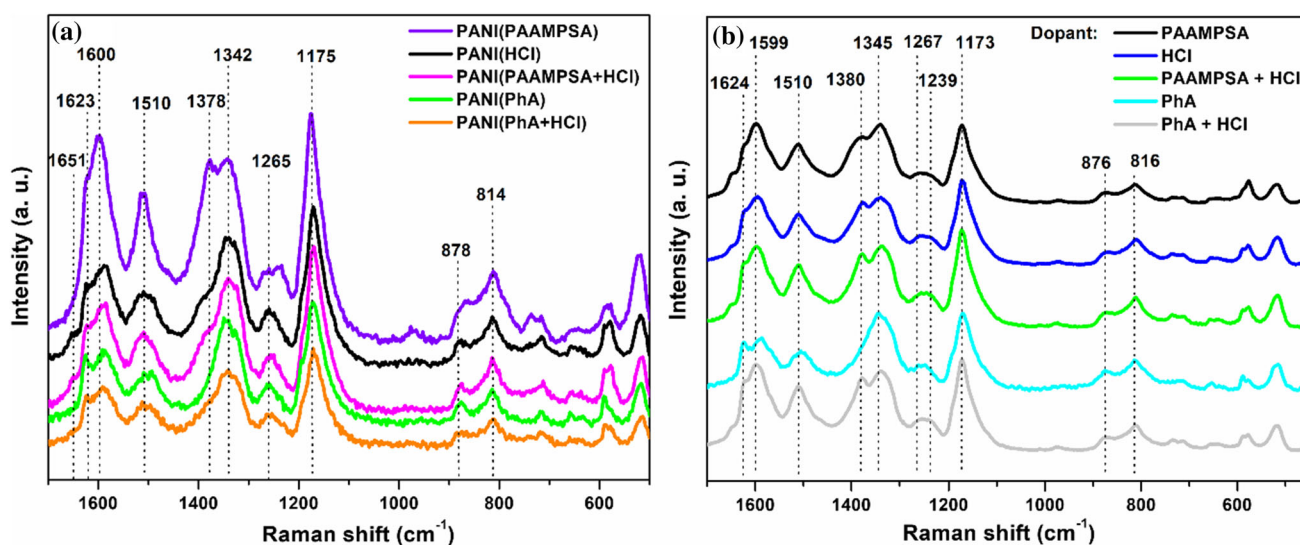
Figure 2 Raman spectra of **a** PANI powders, and **b** PANI-NFC composites prepared with various doping acids.

semiquinonoid units), 878 cm^{-1} (C–N–C out of plane wagging and benzene ring deformations) and 814 cm^{-1} (benzene ring deformations) [21, 23, 24]. No structural changes are observed in PANI-NFC composites when compared to the PANI powders regardless of the chemical nature of the doping agent, which is consistent with the formation of emeraldine salt (Fig. 2b).

The redox states and protonation degrees in PANI powders and PANI-NFC composites as a function of the doping acid(s) were assessed by means of XPS analysis [21, 25–27]. High resolution spectra of nitrogen were deconvoluted into their components in order to determine the redox state of PANI and its protonation levels as a function of the doping acid(s). It can be noticed that the N(1 s) core-level spectra in

Figure S1 (see in the supporting information) and Table 1 were deconvoluted into three peaks with maxima at around 399.4 eV, 400.6 eV and 402.3 eV corresponding to nitrogen atoms in secondary amine, semiquinone (delocalized polaron lattice) and protonated imine (localized bipolaron), respectively, with a level of protonation of about 40 ± 5% in all PANI powders, suggesting the formation of PANI emeraldine salt regardless of the doping acid(s). The chemical nature and the proportion of the different chemical states of nitrogen functionalities in PANI-NFC composites evaluated by fitting the N(1 s) core spectra (Figure S2 in supporting information and Table 1) are equivalent to those of their PANI powder analogs. They exhibited a protonation level of 40 ± 5% comparable to that displayed by the PANI

Table 1 Summary of XPS data of as-synthesized materials

|	NH (%)	NH + (%)	NH + = (%)
Binding Energy (eV)	399	400	402
PANI(HCl)	56.9	30.4	12.7
PANI(PAAMPSA)	61.5	29.4	9.1
PANI(PhA)	57.4	30.0	12.6
PANI(PAAMPSA + HCl)	59.5	27.8	12.8
PANI(PhA + HCl)	64.1	24.2	11.7
PANI(HCl)-NFC	60.3	28.4	11.4
PANI(PAAMPSA)-NFC	62.4	23.7	13.9
PANI(PhA)-NFC	65.9	22.0	12.1
PANI(PAAMPSA + HCl)-NFC	53.8	26.7	19.6
PANI(PhA + HCl)-NFC	58.1	30.6	11.3

powders. The formation of doped PANI in PANI-NFC composites is also evident from X-ray diffractograms (Figure S3 in supporting information) where the characteristic peaks at 25.3° and 9.0° are pointed out [28], thus indicating that the crystalline structure of PANI is not influenced by the chemical nature of the doping acids. The characteristic peaks of NFC crystalline structure corresponding to cellulose Iβ are also detected at 15.5°, 16.8°, 20.4°, 22.7° and 34.7° [29]. Therefore, the structural properties revealed by Raman spectroscopy, XPS and XRD indicate that on one hand NFC does not affect the protonation levels of PANI and on the other hand all selected acids act as good doping agents.

Impact of the chemical nature of the doping acid(s) on the morphological and textural features of PANI-NFC composites was examined. SEM pictures of individually and dually doped PANI-NFC composites are shown in Fig. 3. In comparison with the fibrillar morphology of pristine NFC, NFC fibers are thoroughly covered by PANI in all PANI-NFC composites. Apart from this, morphological differences can be observed. While in all composites globular-like morphology of PANI on the surface of NFC fibers is revealed, dissimilarities in the shape of those globules and their compactness at a nano-scale level can be associated with the type of the dopant. The morphology of PANI(HCl)-NFC reveals a high compactness of the globular objects, whereas in PANI(-PAAMPSA)-NFC and PANI(PhA)-NFC a well-defined globular-like objects of about 200 nm on the surface of NFC are formed. Interestingly the morphology of the dually doped PANI-NFC composites PANI(PAAMPSA + HCl)-NFC and PANI(PhA + HCl)-NFC is a result of a combination of the morphologies caused by each individual dopant. Indeed, the surface of NFC fibers in PANI(PAAMPSA + HCl)-NFC and PANI(PhA + HCl)-NFC is covered by much less defined spiky globular-like structures, due to their higher compactness/coalescence as compared to their HCl-free analogs.

This dopant(s)-dependent morphological features observed by SEM are correlated with the textural differences observed between the components as can be seen in Figure S4 and Table 2. Interestingly, based on BET model, all composites exhibited one type of pores with comparable total pore volume, except for PANI(HCl)-NFC. PANI(HCl)-NFC did not display any detectable porosity, hence confirming its high compactness. Nitrogen physisorption isotherms also indicated that the BET surface area (S_{BET}) is the lowest for the composite doped with HCl and the highest for those doped with PhA or PAAMPSA. Intermediate values of S_{BET} were recorded for the dually doped composites. The increase in the S_{BET} in the presence of organic acids can be correlated with the morphological changes induced by the latter. PANI crosslinked with phytic acid can ensure higher S_{BET} [30]. Indeed, being a crosslinker of PANI thanks to the multiple phosphoric acid groups present in its backbone [19], PhA can lead to the formation of well-defined 3D nanostructures and induce porosity [20]. On the other side, owing to its macromolecular structure PAAMPSA can act as side chains when PANI chains are arranged into crystalline structure. PAAMPSA side chains follow the backbone's arrangement and form a layer between the lattices of PANI. This causes the decrease in d-spacing, and thus an increase in the S_{BET} [31]. Both PhA and PAAMPSA acted as secondary dopants in the dually doped composites through the macromolecular rearrangements of PANI chains [12].
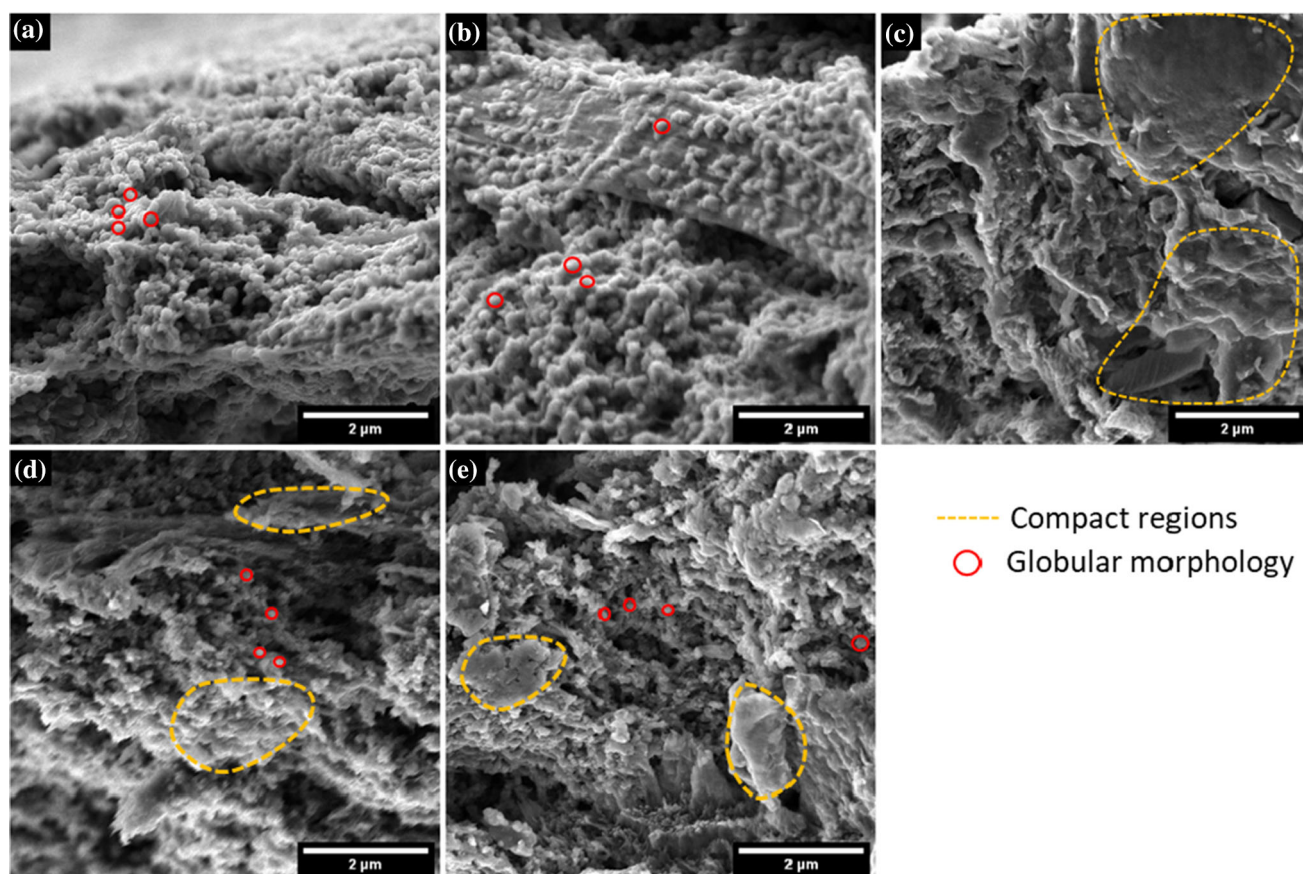
Figure 3 SEM micrographs of PANI-NFC composites doped with various acids: **a** PANI(PAAMPSA)-NFC, **b** PANI(PhA)-NFC, **c** PANI(HCl)-NFC, **d** PANI(PhA + HCl)-NFC, and **e** PANI(PAAMPSA + HCl)-NFC.

**Table 2** Textural properties of PANI-NFC composites doped with various acids

Sample name	S_{BET} $(m^2 \cdot g^{-1})$	Total pore volume $(cm^3 \cdot g^{-1})$
PANI(PAAMPSA)-NFC	17.8	0.035
PANI(PhA)-NFC	17.5	0.035
PANI(HCl)-NFC	9.4	Low porosity
PANI(PhA + HCl)-NFC	13.7	0.039
PANI(PAAMPSA + HCl)-NFC	13.8	0.043

Electrical and electrochemical properties

PANI-NFC composites doped with weak-organic acids, i.e., PhA and PAAMPSA, display much lower electrical conductivities compared to the solely HCl-doped composite (Fig. 4a). The electrical conductivity is sorted in this direction: PAAMPSA (0.01 S·cm^{-1})- < PhA (0.32 S·cm^{-1}) < HCl (2.43 S·cm^{-1}). The conductivity value of the dually doped PANI-NFC with PhA and HCl (2.28 S·cm^{-1}) is comparable to that of the individually doped PANI-NFC with HCl, thereby indicating that HCl is the main dopant for PANI. Synergistic increase in the conductivity is however observed for dually doped PANI-NFC with the combination of PAAMPSA and HCl (3.43 S·cm^{-1}) compared to the corresponding conductivity values of both individually doped PANI-NFC. This phenomenon of two dopants synergy has been already described in literature for pristine PANI [10–12], but no mechanism explaining this phenomenon has been established yet. According to Bhandari et al. [10, 11], a variation of charge densities takes place along the
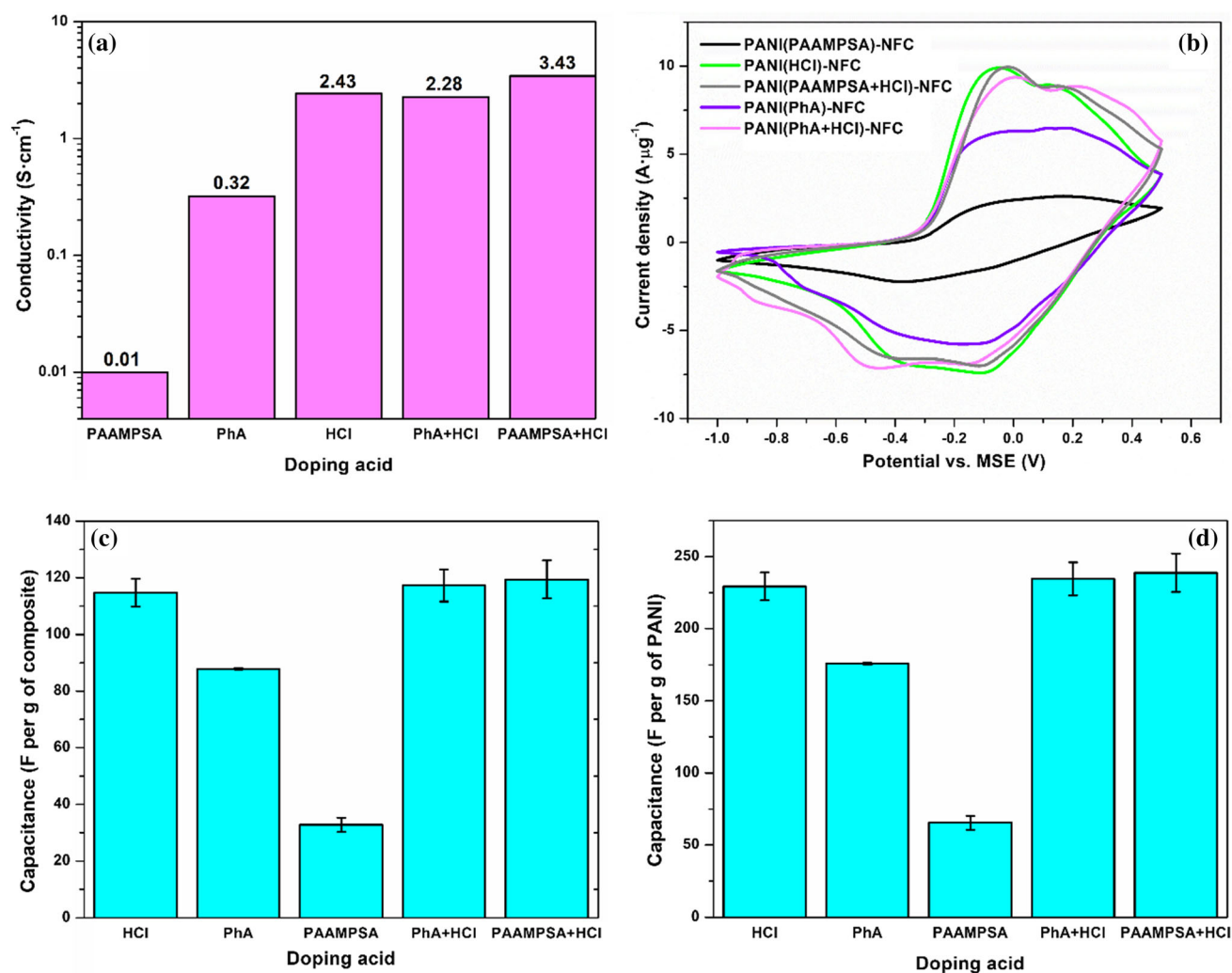
Figure 4 **a** Electrical conductivities, **b** cyclic voltammograms of the composite films in 1 M H_2SO_4 at 50 mV·s^{-1} scan rate, **c** specific capacitances in F per g of composite, and **d** specific capacitances in F per g of PANI evaluated from CV measurements of PANI-NFC composites doped with various acids.

PANI chains when two doping acids are used, thus facilitating intermolecular charge transport. Nonetheless, this hypothesis has not been further verified. Another hypothesis described by MacDiarmid et al. is based on the concept of secondary doping [12]. A secondary dopant is an apparently inert substance (e.g., solvent) that increases the resulting conductivity of already doped conductive polymer. The secondary dopant causes conformational changes in the polymer, which result in enhancement of conductivity through more effective π-conjugation. When secondary dopant is removed from the system, the changes persist. In our composites, the role of the secondary dopant would be taken by PAAMPSA. Unlike PhA, the conformational changes induced by

PAAMPSA are probably more favorable for the enhancement of conductivity through more effective π-conjugation [31]. Indeed, as above mentioned, it is well-known that PAAMPSA can affect the crystalline morphology of PANI owing to its macromolecular structure, low glass transition temperature, and acidic nature. [21, 32]. PAAMPSA can act as side chains when PANI chains are arranged into crystalline structure. PAAMPSA side chains follow the backbone's arrangement and form a layer between the lattices of PANI, [31] which could promote molecular conformation changes of PANI from compact coil to expanded coil. [12]. In PANI(-PAAMPSA + HCl)-NFC, morphological and textural changes of PANI induced by the secondary dopant,

i.e., PAAMPSA through the macromolecular rearrangements of PANI chains was followed by the enhancement of the electrical conductivity. The electrical conductivity enhancement cannot be attributed to a higher degree of doping in the presence of PAAMPSA + HCl since XPS analysis clearly showed that all composites exhibited similar protonation level around 40% whatever the nature of the dopant. Therefore, it is more likely that the macromolecular rearrangements of PANI chains induced by PAAMPSA was responsible for the conductivity enhancement through more effective π-conjugation in PANI expanded coil as supported by the studies of MacDiarmid et al. [12]

The electrochemical behavior of PANI-NFC composites analyzed by cycling voltammetry (CV) is illustrated in Figure S5 and Fig. 4b, c and d. Qualitatively, the cyclovoltammograms of PANI-NFC composites and PANI powders are different (Figure S5). PANI powder-based electrodes show all the characteristic peaks of PANI: transition between leucoemeraldine and emeraldine (R1 and O1) at lower potentials between – 1.0 and 0.0 V vs. MSE and also transition between emeraldine and pernigraniline (R2 and O2) at higher potentials between 0.2 and 0.5 V vs. MSE and broad oxidation and reduction peaks (R3 and O3) around 0.0 V vs. MSE indicating quinone/hydroquinone redox switching [33]. On the contrary, in the case of PANI-NFC composites, the current peaks are much less pronounced and convoluted together. This most likely relates to the more complex 3D structure of the composite since PANI redox switching is controlled by the diffusion of acid molecules from the electrolyte bulk, the porous structure hindering the mass transport can result in a non-homogeneous potential distribution and broader current peaks [34]. Redox potential distribution can be also caused by interactions among the redox centers [34, 35], in this case, NFC could be mediating a specific chemical environment that can promote different interactions among the PANI chains. The electrochemical performance of all PANI-NFC composites is depicted in Fig. 4b, c and d. As can be observed, all three composites that contain HCl (i.e., PANI(HCl)-NFC, PANI(PhA + HCl)-NFC and PANI(PAAMPSA + HCl)-NFC) as a dopant reach very similar peak current densities in the CV experiments and thus equivalent specific capacitances of ∼ 120 F per g of composite. The synergetic improvement in the electrical conductivity observed

for the composite doped with PAAMPSA + HCl is not reflected in the pseudocapacitive behavior of the latter. On the other hand, the composites doped solely with PAAMPSA or PhA exhibited inferior specific capacitance, i.e., ∼ 33 and 88 F per g of composite, respectively. These results indicate that the specific capacitances of the composites are correlated with the doping strength of the individual acids [36, 37]. The morphological and textural features induced by the secondary dopants (PAAMPSA or PhA) by the enhancement of the S_{BET} do not affect the specific capacitances of the composites (see Fig. 4c and d and Table 2). The textural changes induced by the secondary dopant are probably not sufficient (i.e., S_{BET} is not substantially increased) to affect the electrochemical properties. Based on the rational screening of a suitable doping acid for PANI in PANI-NFC composites, the combination of a polymeric acid, i.e., PAAMPSA, with strong inorganic acid, i.e., HCl, is optimal as HCl confers to the composite higher conductivity while PAAMPSA allows improving the mechanical properties, the dispersibility in water besides its ability to protonate PANI even in media of higher pH [38, 39].

PANI-based composites doped with PAAMPSA-HCl: impact of the composition

Chemical structure and morphology

The effect of mass ratio between PANI and cellulose matrices (i.e., NFC or CNFC) on the chemical structure of PANI was examined by Raman spectroscopy (Fig. 5a and b) and XPS (Figure S6 and Figure S7). All composites (PANI(PAAMPSA + HCl)-NFC and PANI(PAAMPSA + HCl)-CNFC) at different ratios PANI to NFC or CNFC exhibited very similar spectral features in accordance with the formation of emeraldine salt. According to the deconvolution of the N(1 s) core level spectra (Figure S6 and Table 3), all composites exhibited a protonation level of 40 ± 5% comparable to that of PANI(PAAMPSA + HCl) powder. Interestingly, the deconvolution of the C(1 s) core level spectra for all composites (Figure S7 and Table S2) show that the proportion of C–O/C–N at 286.5 eV is the highest (i.e., 44 ± 3%) in the composites containing the lowest content of PANI(PAAMPSA + HCl), i.e., 40 wt%. At higher PANI(PAAMPSA + HCl) content (≥ 50 wt%), the
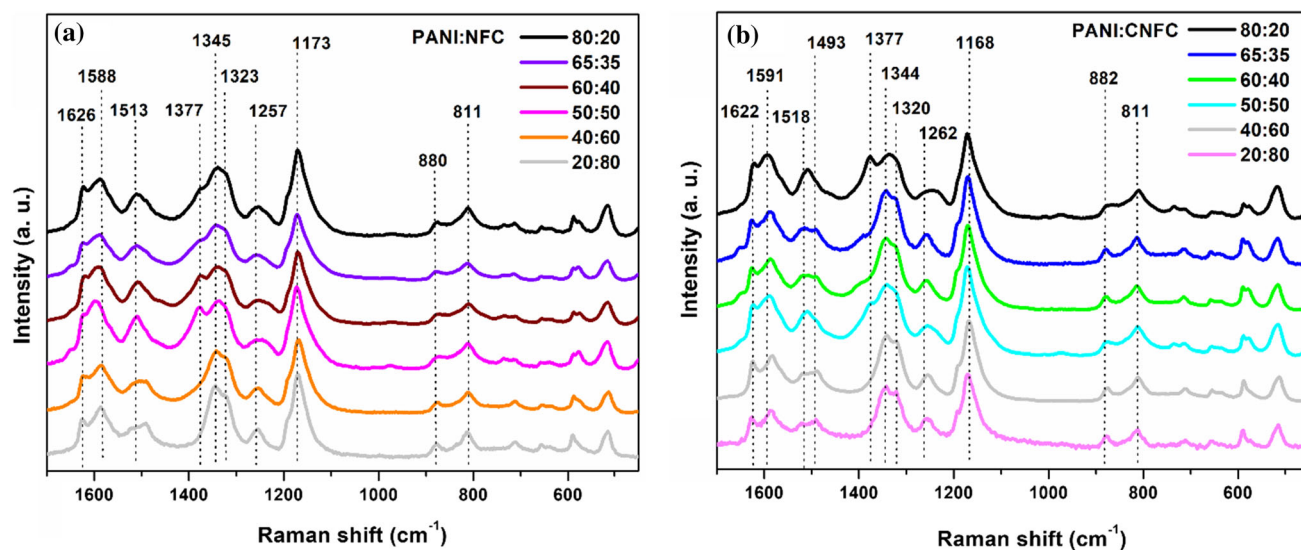
Figure 5 Raman spectra of **a** PANI-NFC, and **b** PANI-CNFC composites doped with PAAMPSA-HCl at different PANI to NFC or CNFC ratios.

Table 3 Summary of XPS data of as-synthesized materials

	NH (%)	NH + (%)	NH + = (%)
Binding Energy (eV)	399	400	402
PANI(PAAMPSA + HCl)-NFC_40:60	62.7	18.4	19
PANI(PAAMPSA + HCl)-CNFC_40:60	58.5	20.4	21.1
PANI(PAAMPSA + HCl)-NFC_50:50	53.8	26.7	19.6
PANI(PAAMPSA + HCl)-CNFC_50:50	63.4	21.0	15.6
PANI(PAAMPSA + HCl)-NFC_60:40	57.6	25.5	16.9
PANI(PAAMPSA + HCl)-CNFC_60:40	60.4	21.9	17.8
PANI(PAAMPSA + HCl)-NFC_65:35	66.3	23.6	10.1
PANI(PAAMPSA + HCl)-CNFC_65:35	59.5	25.9	14.6
PANI(PAAMPSA + HCl)-NFC_80:20	59.4	27.5	13.2
PANI(PAAMPSA + HCl)-CNFC_80:20	55.9	24.4	19.7

proportion of C–O/C–N remains constant at $24 \pm 3\%$. The decrease in the amount of C–O/C–N with the increase in PANI loading correlates with a higher coverage of the surface of NFC or CNFC with PANI since a significant proportion of C–O/C–N can come from NFC or CNFC surface if the latter is not fully covered like in the case of PANI(PAAMPSA + HCl)-NFC at a ratio of 40:60. The maximum coverage of the surface of NFC or CNFC is achieved at a content of PANI(PAAMPSA + HCl) higher or equal to 50 wt.%. As a consequence of the surface oxidation of CNFC, an additional peak appeared at 189 eV corresponding to –COOH after deconvolution of the C(1 s) core level spectra for PANI(PAAMPSA +

HCl)-CNFC composites. In short, the polymerization of PANI in the emeraldine salt form is not affected by the carboxylation of the NFC fibers.

SEM images of PANI(PAAMPSA + HCl)-NFC and PANI(PAAMPSA + HCl)-CNFC composites are shown in Figs. 6 and 7, respectively. Globally, the composites prepared from CNFC have a more compact structure compared to their NFC-based counterparts. This morphology is a result of the defibrillation of cellulose fibers after TEMPO oxidation treatment as evidenced by TEM analysis. (Figure S8). TEM images highlight a finer structure and higher degree of defibrillation in CNFC compared to NFC. This was corroborated by the excellent colloidal
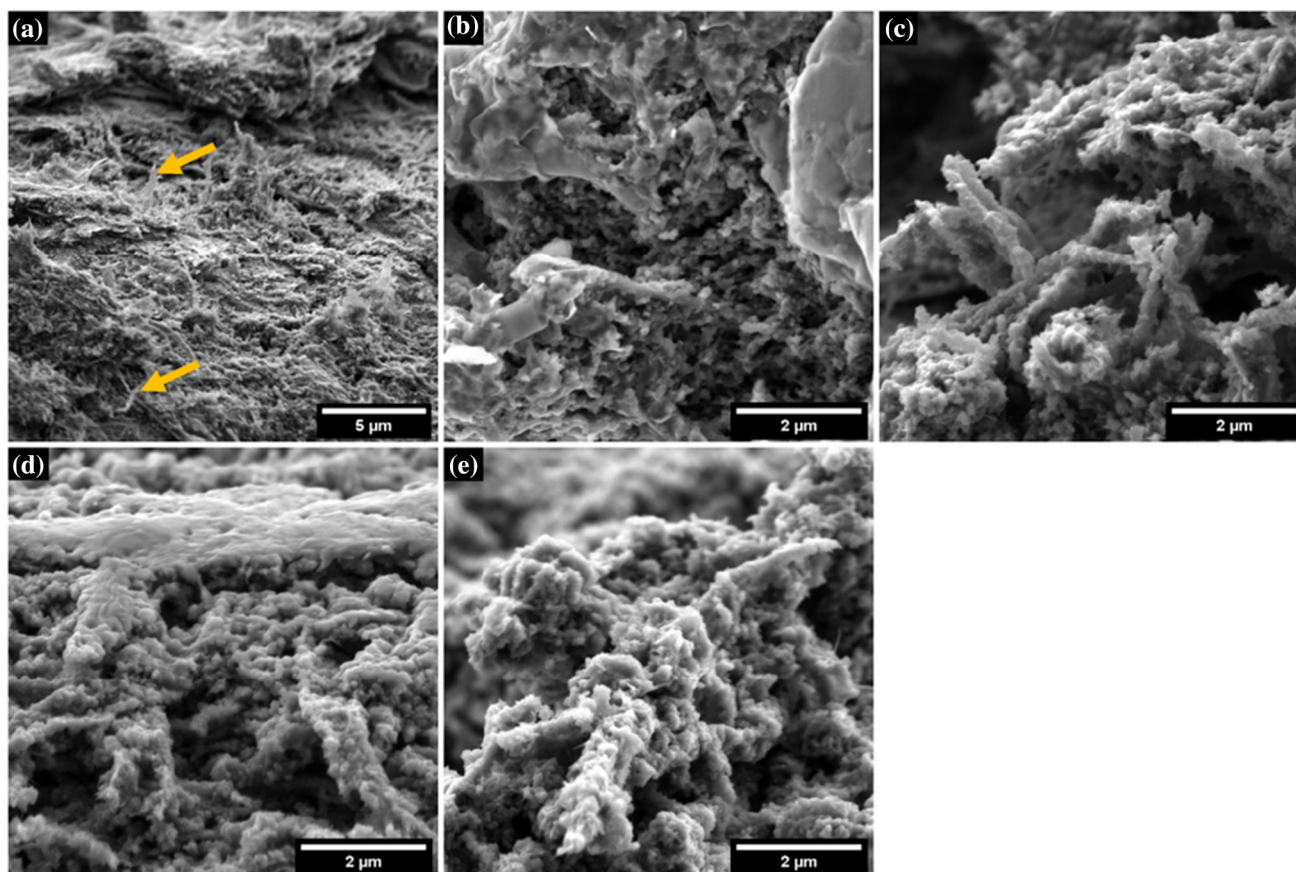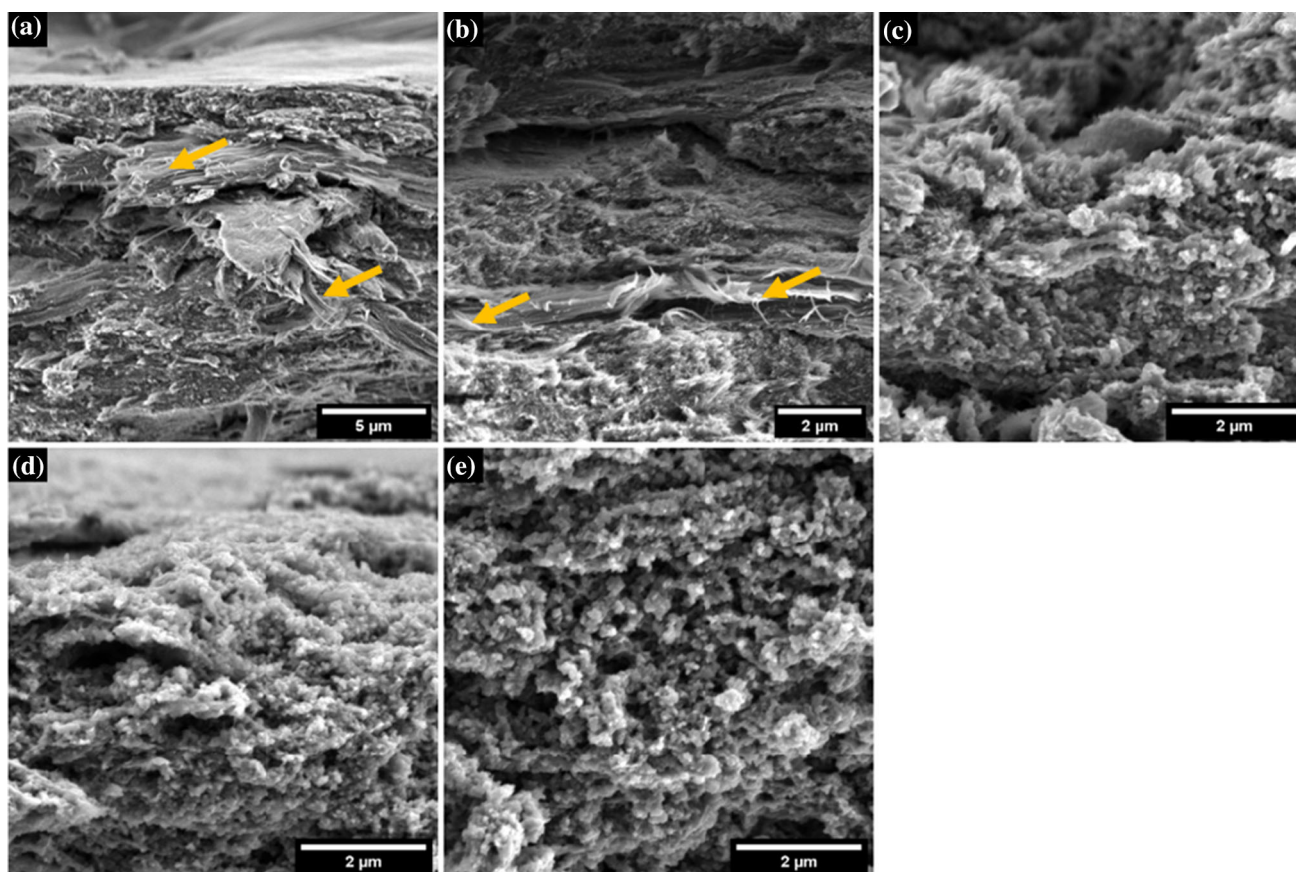
Figure 6 The SEM micrographs of PANI(PAAMPSA + HCl)-NFC composites at a ratio PANI to NFC: **a** 40:60, **b** 50:50, **c** 60:40, **d** 65:35 and **e** 80:20. ⟵——— : The arrows point to the presence of naked cellulosic fibers in some composites.

stability of CNFC in aqueous medium. Consequently, the spiky globular-like structures of PANI(PAAMPSA + HCl) covering CNFC are smaller and the coating layer is finer than in the case of NFC. As a consequence of this morphology, the S_{BET} is close to zero in the composites prepared from CNFC (Table 4) unlike those processed from NFC. NFC-based composites show much more prominent fibrillar morphology with cellulose fibrils covered by globular-like structures of PANI(PAAMPSA + HCl) layer.

At lower amount of PANI(PAAMPSA + HCl) (i.e., $\leq$ 50 wt% PANI(PAAMPSA + HCl)), naked cellulosic fibers are visible in both types of composites. These morphological observations are in a good agreement with XPS results. S_{BET} of NFC-based composites increases with the increase in PANI(PAAMPSA + HCl) content up to 50 wt%., which corresponds to the maximum coverage of NFC surface.

Electrochemical behavior of PANI(PAAMPSA + HCl)-NFC and PANI(PAAMPSA + HCl)-CNFC composites

Electrochemical behavior of PANI(PAAMPSA + HCl)-NFC and PANI(PAAMPSA + HCl)-CNFC composites as a function of the composition is illustrated in Fig. 8. Cyclic voltammetry was carried out in a three-electrode setup measurement at 50 mV·s^{-1} scan rate to evaluate the effect of ratios between PANI and NFC in the prepared composites on their charge storage properties. The results are summarized in the histograms (Fig. 8a). According to expectations the capacitance per gram of the whole composite shows an increasing trend with decreasing amount of NFC, which is consistent with the fact that each composite contains the same mass of PANI (thus, wt. ratio of PANI:NFC increases). An interesting conclusion can be drawn from the results when the values of capacitances are taken relative to the

Figure 7 The SEM micrographs of PANI(PAAMPSA + HCl)-CNFC composites at a ratio PANI to CNFC: **a** 40:60, **b** 50:50, **c** 60:40, **d** 65:35 and **e** 80:20. ⟵⟵⟵ : The arrows point to the presence of naked cellulosic fibers in some composites.

Table 4 Textural properties of PANI(PAAMPSA + HCl)-NFC and PANI(PAAMPSA + HCl)-CNFC composites

Sample name	S_{BET} (m^2·g^{-1})
PANI(PAAMPSA + HCl)-NFC_40:60	5.0
PANI(PAAMPSA + HCl)-NFC_50:50	13.8
PANI(PAAMPSA + HCl)-NFC_60:40	13.5
PANI(PAAMPSA + HCl)-CNFC_50:50	0.5

mass of PANI as is shown in Fig. 8b. It is clear that the charge storage properties of these composites are not influenced by the amount of cellulose matrices or the type of the matrix in case of all composites, except for the samples with lowest loading of PANI. In other words, the degree of PANI utilization is comparable for all composites. This trend can be connected to the surface coverage of the cellulose fibers with PANI. The comparison of the electrochemical results with nitrogen physisorption isotherms (Table 4) suggest that there is no correlation between S_{BET} evaluated

from physisorption measurements and capacitance. According to BET, PANI(PAAMPSA + HCl)-CNFC_50:50 is a very compact and non-porous material (with low S_{BET} of 0.5 m^2·g^{-1}) while its capacitance is comparable to more porous films based on non-carboxylated NFC with much higher S_{BET} (such as PANI(PAAMPSA + HCl)-NFC_50:50 providing 13.8 m^2·g^{-1}). This can mean that the charge storage occurs at the superficial layer of the composite and that the bulk is not utilized in any way, probably because of the non-porosity of the
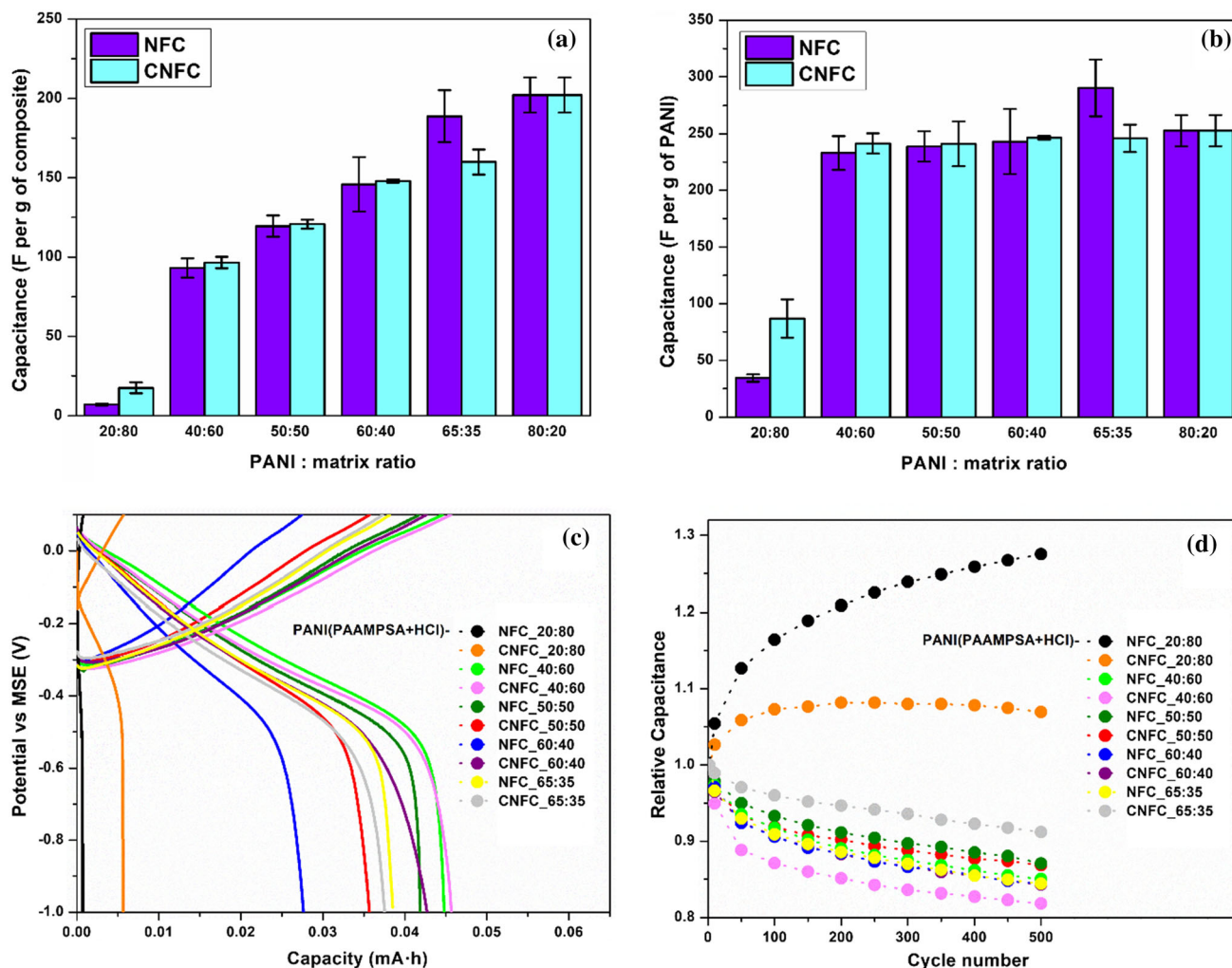
Figure 8 **a** The specific capacitances in F per g of composite evaluated from CV measurements at 50 mV·s^{-1} for various PANI/NFC or CNFC ratios; **b** specific capacitances in F per g of PANI evaluated from the CV measurements at 50 mV·s^{-1} for various PANI/NFC or CNFC ratios; **c** potential dependence on charge–discharge capacity evaluated from GCD experiments at 0.64 mA·cm^{-2} in the potential window from − 1 V to 0.1 V vs. MSE; **d** Relative specific capacitance of the composite films as a function of the number of cycles evaluated form the GCD experiments.

composites according to the nitrogen physisorption isotherms. Therefore, incomplete surface coverage of NFC or CNFC fibers would lead to decrease in charge storage capability. However, we have to be aware that the S_{BET} values for all the composites are relatively small when compared to standard supercapacitive electrodes based on activated carbons [40]. The enhancement in electrode–electrolyte area (e.g., by incorporation of high surface area carbon fillers), thus can be used to increase the charge storage capacity of the material.

The mid-term cycling stability of the composites upon the simulated electrochemical load was probed by GCD experiments in three-electrode set-up. The composites were subjected to 500 cycles at controlled current of 2 mA (corresponding to current density of 0.64 mA·cm^{-2}) in a potential window from − 1 to 0.1 V vs. MSE. The used potential window encompasses only the leucoemeraldine-emeraldine redox transition to avoid excessive composite degradation by hydrolysis of PANI. An example of a charging–discharging curve that was used for capacitance evaluation can be seen in Fig. 8c. The charge–discharge plateaus corresponding to redox transition are located in the potential range between 0.1 and – 0.5 V vs. MSE, which is in good agreement with the CV
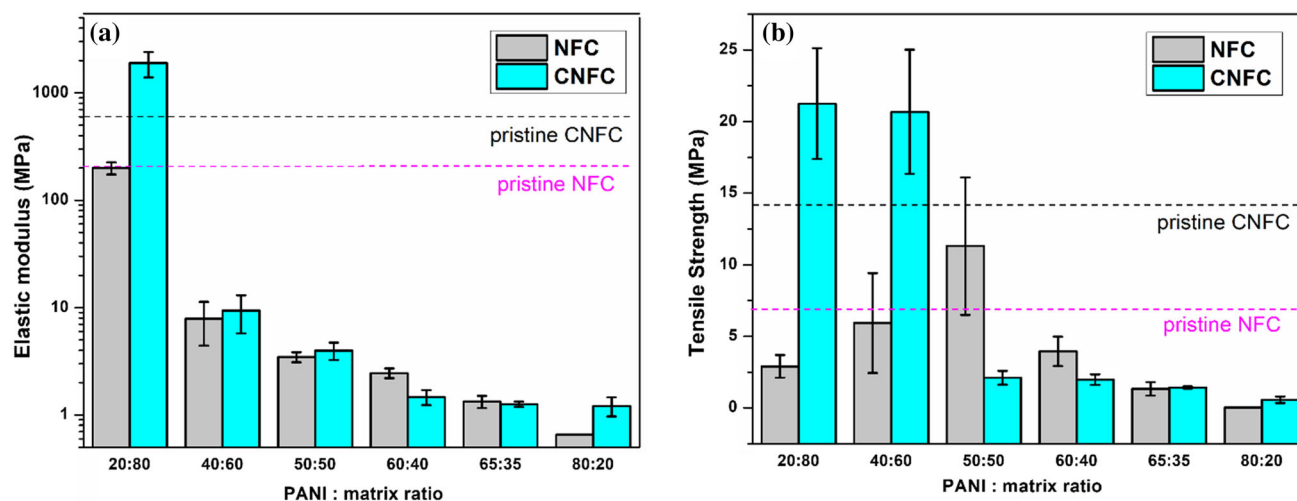
Figure 9 **a** Elastic modulus and **b** ultimate tensile strength of PANI(PAAMPSA + HCl)-NFC and PANI(PAAMPSA + HCl)-CNFC composites at various PANI to NFC or CNFC ratios as a function of composition.

measurements (Fig. 4). The evolution of capacitance for the composites is depicted in Fig. 8d. All composites, except for those with the lowest loading of PANI, show very similar cycling stability–after 500 cycles, the capacitance decreased by about 15% of the initial value. Interestingly, composites with the lowest loading of PANI show an increasing trend of capacitance with number of cycles. This phenomenon could be caused by the inhomogeneity of the composite. Incomplete coverage of the fibers with PANI exposes the highly hydrophilic cellulose to the aqueous electrolyte. Gradual wetting of the fibers can then lead to exposing more of the PANI to the electrolyte, thus increasing the PANI utilization and, in turn, the capacitance of the film.

Mechanical properties of PANI(PAAMPSA + HCl)-NFC and PANI(PAAMPSA + HCl)-CNFC composites

Enhanced mechanical strength and elastic modulus are displayed by the composites with the increased loading of NFC or CNFC as can be seen in Fig. 9 thanks to the outstanding mechanical features of NFC and CNFC. For instance, the composites containing more than 50 wt% NFC or CNFC loading exhibited the highest tensile strength and elastic modulus. In this loading range, CNFC-based composites displayed improved mechanical properties compared to their NFC analogs, thanks to the finer structure and higher degree of defibrillation of CNFC after TEMPO oxidation treatment (Figure S8). In

addition, all composites containing higher than 35 wt% loading of NFC or CNFC can be readily rolled up thanks to their high flexibility as both cellulosic matrices act as a mechanical skeleton capable of high deformations. Abundant hydroxyl and carboxylate groups present on the surface of NFC or CNFC can interact with PANI, and hence may be responsible for the enhancement in the mechanical properties of the composites.

Conclusions

The present study shed the light on the effect of the dual doping of PANI chains via combination of primary (HCl) and secondary (PhA or PAAMPSA) dopants in NFC-based flexible pseudo-capacitor electrodes on the morphological, textural and related electrical and electrochemical properties. Both PhA and PAAMPSA induced morphological and textural changes (increase in the S_{BET}) in the dually doped PANI-NFC composites. Synergistic increase in the electrical conductivity in the case of the dually doped PANI-NFC with PAAMPSA and HCl (i.e., PANI(PAAMPSA + HCl)-NFC) was correlated with a more favorable morphological changes in the composites. Interestingly, the morphological and textural features induced by the secondary dopants (PAAMPSA and PhA) by the enhancement of the specific surface area do not significantly affect the capacitances of the composites evaluated from electrochemical

measurements. These were rather correlated with the doping strength of the individual acids. Despite the significant difference in their S_{BET}, the electrochemical behavior of the composites PANI(PAAMPSA + HCl)-NFC and PANI(PAAMPSA + HCl)-CNFC were comparable and the utilization of PANI for charge storage was not significantly affected by the composition of the film (weight ratio of the constituents) or nature of NFC matrix. While the TEMPO oxidation of NFC surface (i.e., CNFC) does not affect the electrical and the electrochemical performance of the dually doped composite films, it does enhance the mechanical properties of the latter by acting as a mechanical skeleton capable of higher deformations as compared to NFC.

Acknowledgements

Declarations

Conflict of interest   There are no conflicts to declare.

Supplementary Information: The online version contains supplementary material available at https://doi.org/10.1007/s10853-022-07491-3.

References

[1] Nyholm L, Nystrom G, Mihranyan A, Stromme M (2011) Toward flexible polymer and paper-based energy storage devices. Adv Mater 23(33):3751–3769

[2] Nishide H, Oyaizu K (2008) Toward flexible batteries. Science 319(5864):737–738

[3] Du X, Zhang Z, Liu W, Deng Y (2017) Nanocellulose-based conductive materials and their emerging applications in energy devices–A review. Nano Energy 35:299–320

[4] Moon RJ, Martini A, Nairn J, Simonsen J, Youngblood J (2011) Cellulose nanomaterials review: structure, properties and nanocomposites. Chem Soc Rev 40(7):3941–3994

[5] Siqueira G, Bras J, Dufresne A (2010) Cellulosic bio-nanocomposites: a review of preparation properties and applications. Polymers 2:728–765

[6] Snook GA, Kao P, Best AS (2011) Conducting-polymer-based supercapacitor devices and electrodes. J Power Sources 196(1):1–12

[7] Yan H, Chunyi Z (2017) Functional flexible and wearable supercapacitors. J Phys D Appl Phys 50(27):273001

[8] Wang Z, Carlsson DO, Tammela P, Hua K, Zhang P, Nyholm L, Strømme M (2015) Surface modified nanocellulose fibers yield conducting polymer-based flexible supercapacitors with enhanced capacitances. ACS Nano 9(7):7563–7571

[9] Zheng W, Lv R, Na B, Liu H, Jin T, Yuan D (2017) Nanocellulose-mediated hybrid polyaniline electrodes for high performance flexible supercapacitors. J Mater Chem A 5(25):12969–12976

[10] Bhandari S, Khastgir D (2015) Synergistic effect of simultaneous dual doping in solvent-free mechanochemical synthesis of polyaniline supercapacitor comparable to the composites with multiwalled carbon nanotube. Polymer 81:62–69

[11] Bhandari S, Singha NK, Khastgir D (2013) Electrochemical synthesis of nanostructured polyaniline: heat treatment and synergistic effect of simultaneous dual doping. J Appl Polym Sci 129(3):1264–1273

[12] MacDiarmid AG, Epstein AJ (1995) Secondary doping in polyaniline. Synth Met 69(1):85–92

[13] Yin W, Ruckenstein E (2000) Soluble polyaniline co-doped with dodecyl benzene sulfonic acid and hydrochloric acid. Synth Met 108(1):39–46

[14] Bavio MA, Acosta GG, Kessler T (2014) Synthesis and characterization of polyaniline and polyaniline–Carbon nanotubes nanostructures for electrochemical supercapacitors. J Power Sources 245:475–481

[15] Singu BS, Srinivasan P, Pabba S (2011) Benzoyl peroxide oxidation route to nano form polyaniline salt containing dual dopants for pseudocapacitor. *J Electrochem Soci*, *159*.

[16] Palaniappan S, Devi SL (2008) Novel chemically synthesized polyaniline electrodes containing a fluoroboric acid dopant for supercapacitors. J Appl Polym Sci 107(3):1887–1892

[17] Arenas MC, Andablo E, Castaño VM (2010) Synthesis of conducting polyaniline nanofibers from single and binary dopant agents. J Nanosci Nanotechnol 10(1):549–554

[18] Stejskal J, Gilbert RG (2002) Polyaniline. Preparation of a conducting polymer(IUPAC technical report). Pure Appl Chem 74(5):857–867

[19] Ma Z, Shi W, Yan K, Pan L, Yu G (2019) Doping engineering of conductive polymer hydrogels and their

application in advanced sensor technologies. Chem Sci 10(25):6232–6244

[20] Gawli Y, Banerjee A, Dhakras D, Deo M, Bulani D, Wadgaonkar P, Shelke M, Ogale S (2016) 3D polyaniline architecture by concurrent inorganic and organic acid doping for superior and robust high rate supercapacitor performance. Sci Rep 6:21002

[21] Bautkinová T, Sifton A, Kutorglo EM, Dendisová M, Kopecký D, Ulbrich P, Mazúr P, Laachachi A, Hassouna F (2020) New approach for the development of reduced graphene oxide/polyaniline nanocomposites via sacrificial surfactant-stabilized reduced graphene oxide. Colloids Surf, A Phys Eng Aspects 589:124415

[22] Besbes I, Alila S, Boufi S (2011) Nanofibrillated cellulose from TEMPO-oxidized eucalyptus fibres: effect of the carboxyl content. Carbohyd Polym 84(3):975–983

[23] Trchová M, Morávková Z, Bláha M, Stejskal J (2014) Raman spectroscopy of polyaniline and oligoaniline thin films. Electrochim Acta 122:28–38

[24] Furukawa Y, Ueda F, Hyodo Y, Harada I, Nakajima T, Kawagoe T (1988) Vibrational spectra and structure of polyaniline. Macromolecules 21(5):1297–1305

[25] Jeon JW, Ma Y, Mike JF, Shao L, Balbuena PB, Lutkenhaus JL (2013) Oxidatively stable polyaniline:polyacid electrodes for electrochemical energy storage. Phys Chem Chem Phys 15(24):9654–9662

[26] Vallés C, Jiménez P, Muñoz E, Benito AM, Maser WK (2011) Simultaneous reduction of graphene oxide and polyaniline: doping-assisted formation of a solid-state charge-transfer complex. J Phys Chem C 115(21):10468–10474

[27] Cho S, Lee JS, Jun J, Kim SG, Jang J (2014) Fabrication of water-dispersible and highly conductive PSS-doped PANI/graphene nanocomposites using a high-molecular weight PSS dopant and their application in H2S detection. Nanoscale 6(24):15181–15195

[28] Pouget JP, Jozefowicz ME, Epstein AJ, Tang X, MacDiarmid AG (1991) X-ray structure of polyaniline. Macromolecules 24(3):779–789

[29] French AD (2013) Idealized powder diffraction patterns for cellulose polymorphs. Cellulose 21(2):885–896

[30] Kutorglo EM, Hassouna F, Beltzung A, Kopecký D, Sedlářová I, Šoóš M (2019) Nitrogen-rich hierarchically porous polyaniline-based adsorbents for carbon dioxide (CO2) capture. Chem Eng J 360:1199–1212

[31] Zhang X, Zhu J, Haldolaarachchige N, Ryu J, Young DP, Wei S, Guo Z (2012) Synthetic process engineered polyaniline nanostructures with tunable morphology and physical properties. Polymer 53(10):2109–2120

[32] Chen S-A, Lee H-T (1994) (1994) Structure and properties of poly(acrylic acid)-doped polyaniline. Macromolecules 28:2858–2866

[33] Arsov LD, Plieth W, Koßmehl G (1998) Electrochemical and Raman spectroscopic study of polyaniline; influence of the potential on the degradation of polyaniline. J Solid State Electrochem 2(5):355–361

[34] Costentin C, Porter TR, Savéant J-M (2017) How do pseudocapacitors store energy? theoretical analysis and experimental illustration. ACS Appl Mater Interfaces 9(10):8649–8658

[35] Posadas D, Rodriguez Presa MJ, Florit MI (2001) Apparent formal redox potential distribution in electroactive arylamine-derived polymers. Electrochim Acta 46(26):4075–4081

[36] Motheo AJ, Santos JR, Venancio EC, Mattoso LHC (1998) Influence of different types of acidic dopant on the electrodeposition and properties of polyaniline films. Polymer 39(26):6977–6982

[37] Li X (2009) Improving the electrochemical properties of polyaniline by co-doping with titanium ions and protonic acid. Electrochim Acta 54(24):5634–5639

[38] Nekrasov AA, Gribkova OL, Ivanov VF, Vannikov AV (2010) Electroactive films of interpolymer complexes of polyaniline with polyamidosulfonic acids: advantageous features in some possible applications. J Solid State Electrochem 14(11):1975–1984

[39] Tarver J, Yoo JE, Dennes TJ, Schwartz J, Loo Y-L (2009) Polymer acid doped polyaniline is electrochemically stable beyond pH 9. Chem Mater 21(2):280–286

[40] Zhang X, Zhang H, Lin Z, Yu M, Lu X, Tong Y (2016) Recent advances and challenges of stretchable supercapacitors based on carbon materials. Sci China Mater 59(6):475–494